BIOCHEMISTRY
including biophysical chemistry & molecular biology

Article

pubs.acs.org/biochemistry

Cooperative Binding of PhoB^{DBD} to Its Cognate DNA Sequence—A Combined Application of Single-Molecule and Ensemble Methods

Markus Ritzefeld,[†] Volker Walhorn,[‡] Christin Kleineberg,[‡] Adeline Bieker,[‡] Klaus Kock,[§] Christian Herrmann,[§] Dario Anselmetti,[‡] and Norbert Sewald*[,†]

[†]Organic and Bioorganic Chemistry and [‡]Experimental Biophysics, Bielefeld University, Universitaetsstrasse 25, 33615 Bielefeld, Germany

[§]Physical Chemistry I, Ruhr University Bochum, Universitaetsstrasse 150, 44801 Bochum, Germany

Supporting Information

ABSTRACT: A combined approach based on isothermal titration calorimetry (ITC), fluorescence resonance energy transfer (FRET) experiments, circular dichroism spectroscopy (CD), atomic force microscopy (AFM) dynamic force spectroscopy (DFS), and surface plasmon resonance (SPR) was applied to elucidate the mechanism of protein−DNA complex formation and the impact of protein dimerization of the DNA-binding domain of PhoB (PhoB^{DBD}). These insights can be translated to related members of the family of winged helix-turn-helix proteins. One central question was the assembly of the trimeric complex formed by two molecules of PhoB^{DBD} and two cognate binding sites of a single oligonucleotide. In addition to the native protein WT-PhoB^{DBD}, semisynthetic covalently linked dimers with different linker lengths were studied. The ITC, SPR, FRET, and CD results indicate a positive cooperative binding mechanism and a decisive contribution of dimerization on the complex stability. Furthermore, an alanine scan was performed and binding of the corresponding point mutants was analyzed by both techniques to discriminate between different binding types involved in the protein−DNA interaction and to compare the information content of the two methods DFS and SPR. In light of the published crystal structure, four types of contribution to the recognition process of the *pho* box by the protein PhoB^{DBD} could be differentiated and quantified. Consequently, it could be shown that investigating the interactions between DNA and proteins with complementary techniques is necessary to fully understand the corresponding recognition process.

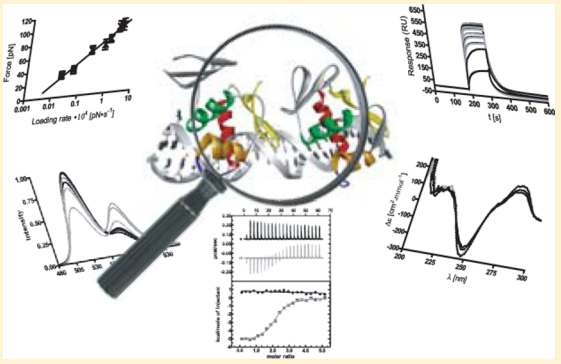

Recognition of particular DNA sequences by proteins is essential for several biological processes including transcription, replication, and recombination. The winged helix-turn-helix (wHTH) motif is a common DNA recognition element in eukaryotes. It comprises a recognition helix (α^3) that mainly interacts with the major groove of the DNA, a second supporting helix that stabilizes the protein−DNA complex (α^2), and a C-terminal β-hairpin (the wing) that penetrates the minor groove of the recognition sequence (cf. Figure 1).[1] Several wHTH transcription factors are homodimers or tetramers that exhibit an exposed patch of hydrophobic residues that mediate protein−protein interactions.[2,3] PhoB is the response regulator of the two-component regulatory system (TCRS) PhoB/PhoR in *Escherichia coli* (*E. coli*). At least 287 genes are differentially expressed in the presence of active PhoB. These genes are involved in all areas of the cellular metabolism, ranging from DNA replication to lipid metabolism.[4] However, only 50 genes are directly regulated by the transcription activator.[5−7] Seven out of the 287 genes encode other transcriptional regulators that transduce the signal of phosphate starvation further downstream.[4] In conclusion, PhoB can be characterized as a global regulator. It is composed of two different domains, the

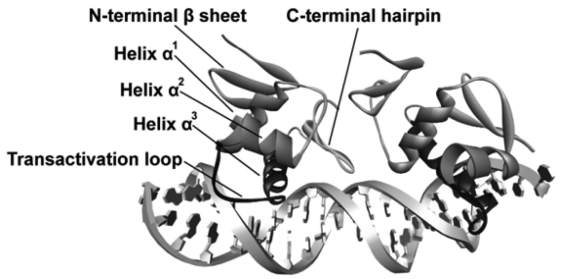

Figure 1. Crystal structure of two PhoB^{DBD}-proteins bound to a *pho* box in a head-to-tail arrangement.[1]

N-terminal regulatory domain (PhoBRD, residues 1−127) and the C-terminal DNA-binding domain (PhoB^{DBD}, residues 127−229).[8] Unlike other representatives of the family of wHTH proteins, the DBD contains a flexible loop (transactivation loop) instead of the typical turn motif.[1,9] Interactions between

Received: June 11, 2013
Revised: October 18, 2013
Published: October 22, 2013

the σ^{70}-subunit of the bacterial RNA polymerase (RNAP) and the transactivation loop and helices α^2 and α^3 of PhoB^{DBD} facilitate a recruitment of the RNAP.[10] In addition, PhoB^{DBD} remodels the σ_4-domain of the σ^{70}-subunit and thereby leads to transcription initiation by favoring the RNA-transcript release.[11] The second component of the TCRS, the inner-membrane histidine kinase PhoR, phosphorylates and thereby activates PhoB when the environmental phosphate concentration declines below a threshold of 4 μM.[8]

In the inactive state, PhoB exists in a monomer−dimer equilibrium where the DBDs of the corresponding dimers point toward opposite directions. Phosphorylation of PhoB in the regulatory domain (PhoBRD) extensively shifts the equilibrium to the dimeric form and results in a structural change where the two DBDs are arranged in a parallel head-to-tail fashion.[12,13] This alteration enables the transcriptional activator to bind to the *pho* box, a DNA sequence located 10 nucleotides upstream of the −10 region in the regulon *pho*. The *pho* box consists of two TGTCA-motifs each of them followed by an A/T-rich sequence.[8,14] If the regulatory domain of PhoB is removed, PhoB^{DBD} still recognizes specifically the DNA on its own and can act as a constitutive activator.[15] Although the PhoBRD domain primarily mediates the formation of PhoB-dimers, extensive protein−protein interactions are also present in the corresponding heterotrimeric complexes consisting of two PhoB^{DBD} and a *pho* box.[1] In conclusion, dimerization seems to influence the recognition of the *pho* box by the isolated DBD, too. We previously communicated binding studies of peptide and protein epitopes of the DBD of PhoB to the *pho* box using atomic force microscopy (AFM) dynamic force spectroscopy (DFS) to quantify the protein−DNA interactions on a single-molecule level (Review concerning AFM based DFS[16]). The quantitative DFS analysis provided force-related properties and kinetic data such as the thermal dissociation rate constant of the wild type PhoB^{DBD}. Moreover, an alanine scan of the three amino acids R193, H198, and R203 was performed. R193 and H198 interact with the TGTCA motif and R203 binds to the backbone of the A/T-rich DNA-region. The results revealed subtle differences between the three epitopes that could not be determined by other methods at this level.[17] We also reported on the specific recognition of different oligonucleotides by PhoB^{DBD} in real-time using SPR (Review concerning SPR [18]).[14] DNA duplexes of different lengths containing one or two TGTCA-motifs based on the *pst*-regulon and oligonucleotides with recognition sequences based on different *pho*-regulons were investigated. All results revealed that both regions of the binding site, the TGTCA-motif and the A/T-rich minor groove, are essential for the overall recognition process. Additionally, the comparison of the *pho*-regulons indicated the dependence of the binding affinity on the base composition of the minor groove.

Here we focus on the binding mechanism and the impact of the formation of PhoB^{DBD}-dimers. Although dimerization seems to influence the recognition of the *pho* box by the pure DBD, the mechanism of the complex assembly is still under debate. In this study, the interaction between the DBD of the transcription factor PhoB and its cognate DNA recognition sequence was investigated by combining different real-time methods to elucidate the binding mechanisms of PhoB^{DBD} and to quantify the impact of protein dimerization on the recognition process. Furthermore, the contribution of certain amino acids to the overall complex stability was analyzed by DFS and SPR to discriminate between different binding types involved in the protein−DNA interaction and to compare the information content of both methods. These insights are expected to be relevant also to related members of the family of winged helix-turn-helix proteins.

EXPERIMENTAL PROCEDURES

Enzymes used for DNA modification, chitin beads and *E. coli* strains were purchased from New England Biolabs (Frankfurt a.M., Germany). All primers and oligonucleotides were purchased from Eurofins MWG Operon (Ebersberg, Germany). Chemicals were obtained from Sigma-Aldrich (Hamburg, Germany), Acros (Geel, Belgium), or Applichem (Darmstadt, Germany). All amino acids and resins were purchased from Iris Biotech GmbH (Marktredwitz, Germany) or Orpegen (Heidelberg, Germany). Atto 550 maleimide was purchased from ATTO-TEC (Siegen, Germany) and the labeling reaction was performed as described in the manual. Analytical RP-HPLC was carried out on a Fisher Scientific Accela system, equipped with a Fisher Scientific Hypersil GOLD 3 μm C18 175 Å column (150 mm × 2.1 mm). Preparative RP-HPLC was performed on a Hitachi MERCK LaChrom system equipped with a Vydac high-performance guard column (C18) and a Phenomenex Jupiter 10 μm C18 300 Å column (250 mm × 4.6 mm). An ÄKTA Explorer 10 system (GE Healthcare, Munich, Germany) equipped with a Superdex 75 10/300 GL (GE Healthcare, Munich, Germany) at a flow of 0.5 mL min^{-1} using phosphate buffer (50 mM Na_2HPO_4, 150 mM NaCl, pH 7.4) was used for preparative gel filtration. MALDI-ToF mass spectra were recorded on a Voyager DE instrument (PerSeptiveBiosystems, Weiterstadt, Germany) with sinapinic acid as the matrix. Prior to measurement, protein samples were desalted using ZipTips (Millipore, Schwalbach, Germany). Protein concentrations were determined from the absorbance at 280 nm (Nanodrop 1000, Thermo Scientific, Bonn, Germany). The High Resolution Mass Spectroscopy (HRMS) experiment was performed on a Fourier Transform Ion Cyclotron Resonance (FT-ICR) mass spectrometer APEX III (Bruker Daltonik, Bremen, Germany) equipped with a 7.0 T, 160 mm bore superconducting magnet (Bruker Analytik GmbH − Magnetics, Karlsruhe, Germany), infinity cell, and interfaced to an external (nano)ESI or MALDI ion source. Scan accumulation and Fourier transformation was done with XMASS NT (7.08). For further data processing DataAnalysis 3.4 was used.

Peptide Synthesis of H-Cys-Lys(FAM)-OH. The 2-chlorotrityl resin was loaded with $N(\alpha)$-Fmoc-$N(\varepsilon)$-alloc-L-lysine using the standard procedure (loading: 0.5 mmol g^{-1}). Coupling of Fmoc-glycine and *N-tert*-butoxycarbonyl-*S*-trityl-L-cysteine was performed using the Fmoc strategy on a Liberty microwave synthesizer (CEM, Kamp-Lintfort, Germany) on a 0.1 mmol scale. The following solutions were used for every coupling step: TBTU (5 equiv, 1 mL of a 0.5 M solution), protected amino acid (5 equiv, 2.5 mL of a 0.2 M solution), DIPEA (10 equiv, 0.5 mL of a 2.0 M solution). 20% piperidine in DMF was used as deprotection solution. The following cleavage of the allyloxycarbonyl (Alloc) group was performed manually on resin at RT using 20 mol % of tetrakis(triphenylphosphine)palladium(0) and phenylsilane (24 equiv) in dry dichloromethane under argon atmosphere until a complete conversion was detected by MALDI-ToF MS. Subsequently carboxyfluorescein (CF, 2.5 equiv) was coupled using *N,N′*-diisopropyl-carbodiimide (2.5 equiv) and *N*-hydroxybenzotriazole (2.5 equiv) in DMF under microwave conditions (30 W, 60 °C, 20 min). The reaction was repeated until the conversion was completed. After successful CF coupling, the resin was washed with 20% piperidine in

Table 1. Primer Sequences of the PhoB^{DBD}-Proteins

protein	primer sequence (5′ → 3′)
WT-PhoB^{DBD}	Fw.: GGTGGTCATATGGCGGTGGAAGAGGTGATTGAG
	Rv.: GGTGGTTGCTCTTCCGCAAAAGCGGGTTGAAAAACG
Q135C	GAGGTGATTGAGATGTGCGGATTAAGTCTCGAC
R176A	GAAGACCGCACGGTCGCTGTCCACATTCGTCGC
T217A	TGACCGCATGGTGCAGGCCGTGCGCGGTACAGG
V218A	CGCATGGTGCAGACCGCGCGCGGTACAGGATAT
Y223A	GCGGGTTGAAAAACGAGCTCCTGTACCGCGCAC
CRA-PhoB^{DBD}	Fw.: GCGGGTTGAAAAACGAGCTCCTGTACCGCGCAC
	Rv.: GGTGGTCTGCAGTTAAAAGCGGGTTGAAAAACG
CRA-LEAF-PhoB^{DBD}	ACAACTGCCGTGCCCTGGAGGCCTTTATGGCGGTGGAAG

DMF in between the standard DCM and DMF washing steps. Final cleavage was performed manually with a solution of 2.5% triisopropylsilane, and 95% TFA for 1 h. The resin was filtered off and the volume of the cleavage solution was reduced to 5 mL. Subsequently, the peptide was precipitated using methyl *tert*-butyl ether followed by RP-HPLC purification. HRMS (FT-ICR-MS m/z): $[M+H]^+$ calcd for $C_{30}H_{29}N_3O_9S$: 608.1697, found: 608.1694. $[M+Na]^+$ calcd for $C_{30}H_{29}N_3O_9S$: 630.1517, found: 630.1517; Analytical RP-HPLC: Gradient: 0−5 min 0−100% acetonitrile, 5−6 min 100% H_2O, 6.5 min 100% H_2O, t_r = 2.79 min.

Protein Expression and Purification. Genomic DNA from *E. coli* K12 was extracted using DNeasy Tissue Kit from Qiagen (Hilden, Germany). Afterward, the DBD of PhoB was amplified by polymerase chain reaction, using either the WT-PhoB^{DBD} or the CRA-PhoB^{DBD} primers (cf. Table 1). The fragments were then inserted into a pTwin2 vector either using NdeI and SapI for WT-PhoB^{DBD} or NcoI and PstI for CRA-PhoB^{DBD}. Point mutations were introduced into WT-PhoB^{DBD} and the amino acid sequence H-LEAF-OH was introduced into CRA-PhoB^{DBD} by QuikChange site directed mutagenesis kit (Stratagene, Amsterdam, Netherlands; primer sequences: cf. Table 1). All plasmids were transformed into *E. coli* ER2566 that were grown at 37 °C in LB medium containing 100 μg mL^{-1} ampicillin. Protein expression was induced at OD_{600} = 0.7 by isopropyl-β-D-thiogalactopyranoside (0.5 mM) and the cells were incubated for further 4 h at 32 °C. After having harvested the cells, pellets were resuspended in buffer (20 mM HEPES, 500 mM NaCl, 1 mM EDTA) containing 20 μM phenylmethylsulfonyl fluoride and 0.1% Tween 20. In the case of WT-PhoB^{DBD} and the point mutants, a buffer with a pH of 7.0 was used, and in the cases of CRA-PhoB^{DBD} and CRA-LEAF-PhoB^{DBD}, a buffer with a pH of 8.5 was used. The suspensions were homogenized by French press and the clear supernatant of the lysed cells was loaded on chitin beads (0.5 mL min^{-1}) that were equilibrated with buffer (10 column volumes, 1 mL min^{-1}) at 4 °C before. After washing (10 column volumes, 1 mL min^{-1}), splicing of the intein was induced in the case of WT-PhoB^{DBD} and the point mutants by adding 1 column volume of buffer containing MESNA (50 mM) at pH 8.5, incubation at 4 °C overnight, and elution of the MESNA-thioester; and in the case of CRA-PhoB^{DBD} and CRA-LEAF-PhoB^{DBD}, by adding 1 column volume of buffer with pH = 7.0, incubation overnight at RT, and elution. Success of protein expression and purification was proven by MALDI-ToF MS (cf. S1).

Native Chemical Ligation. Labeling of WT-PhoB^{DBD} and the point mutants with cysteine for the DFS measurements or H-Cys-Lys(FAM)-OH for the fluorescence experiments was performed by native chemical ligation. Cysteine or the cysteine-containing peptide (2 mM) was added to the corresponding protein-MESNA-thioester and the resulting mixture was incubated at 4 °C overnight. All proteins labeled with H-Cys-Lys(FAM)-OH were further incubated in the presence of TCEP (2 mM) and iodoacetamide (2 mM) for 1 h to mask the sulfhydryl group of the newly introduced Cys residue. Subsequently the excess of all reagents was removed by dialysis against phosphate buffer (10 mM Na_2HPO_4, 5 mM NaCl, pH 7.4). Success of the ligation was proven by MALDI-ToF MS (cf. S1).

Preparation of the PhoB^{DBD}-Dimers. To obtain the two PhoB^{DBD}-dimers, IPL was performed by adding either CRA-PhoB^{DBD} or CRA-LEAF-PhoB^{DBD} to the MESNA-thioester of WT-PhoB^{DBD} and incubation of the reaction mixture at 4 °C overnight in the presence of TCEP (2 mM). During the ligation reaction, both dimers precipitated. Urea (8 M), TCEP (2 mM), and iodoacetamide (2 mM) were added to the precipitated products to denature the dimers and to mask the sulfhydryl groups. Dialysis of the protein solutions against phosphate buffer (100 mM Na_2HPO_4, 50 mM NaCl, pH 7.4) was performed to remove the excess of all reagents and to refold the proteins. Afterward, both dimers were purified by preparative gel filtration.

Oligonucleotides. Table 2 contains the sequences of all oligonucleotides. Nomenclature: *M* = major groove (TGTCA-motif), *m* = minor groove (A/T-rich region), *X* = major groove with random sequence, *x* = minor groove with random sequence.

Isothermal Titration Calorimetry. ITC measurements were performed using an Auto-ITC$_{200}$ (GE Healthcare, Munich, Germany). Protein and DNA samples were dialyzed against the same batch of phosphate buffer (100 mM Na_2HPO_4, 50 mM NaCl, pH 7.4) to minimize artifacts due to minor differences of the buffer composition. The sample cell was loaded with 200 μL of 15 μM dsDNA or pure buffer. Titration experiments consisted of 21 injections of a 415 μM WT-PhoB^{DBD} stock solution. After an initial delay of 120 s, the first injection of 0.5 μL with a duration of 1 s was performed, followed by 20 injections with a volume of 1.8 μL, a duration of 3.6 s, and a delay of 180 s between the additions. The measurements were carried out at a stirring rate of 750 rpm and a temperature of 25 °C. The raw data was evaluated with the software MicroCal Origin using a one-site binding model.

CD Spectroscopy and Fluorescence Measurements. All spectra were recorded on a J-810 CD spectrometer (Jasco, Groß-Umstadt, Germany) equipped with a FDCD-404S fluorescence CD accessory using either a 10 × 2 mm quartz cell for fluorescence or a 0.2 mm quartz cell for CD measurements and phosphate buffer (10 mM Na_2HPO_4,

dx.doi.org/10.1021/bi400718r | *Biochemistry* 2013, 52, 8177−8186

Table 2. Sequences of the 5′-Biotin-Labeled, 5′-Thiol-Labeled (268 bp *pstS pho* box) or Unlabeled Oligonucleotides[a]

name	sequence (5′ → 3′)
MmMm	**CTGTCA***TAAAAC***TGTCA***TATTCCT*
MmXx	CTGTCA*TAAAAC*GAGGCAGCATCT
268 bp *pstS pho* box	CGCCAGGGTTTTCCCAGTCACGACGTTGTAAAACGACGGCCAGTGCCAAGCTTACCGTCATCTTCGGC-TACTTTTTCTCTGTCACAGAATGAAAATTTTTCTGTCATCTCTTCGTTATTAATGTTTGTAATTGACTGAATAT-CAACGCTTATTTAAATCAGACTGAAGACTTTATCTCTC**TGTCA***TAAAAC***TGTCA***TATTCC***TTACA***TATAAC***TGT-CAC***CTGTT*TTGTCCTATTTTGCTTCTCGTAGCCAACAAACAATGCTTTATGAATCCTCCCAGGAGACATTATGAAAGT-TATGCGTACCACCGTCGAATTCGTAATCATGGTCATAGCTGTTTCCTGTGTGAAATTGTTATCCGCT

[a]The TGTCA-motif is printed in bold and the A/T-rich region in italics.

5 mM NaCl, pH 7.4). The CD spectra were recorded at room temperature at a scanning rate of 50 nm × min^{-1}, a data pitch of 0.2 nm, three accumulations, and a protein concentration of 12 μM. Temperature dependent CD spectra were recorded between 20 and 75 °C with a temperature gradient of 1 °C min^{-1}, a delay time of 1 min, a data pitch of 2 °C, and a protein concentration of 12 μM. In order to analyze structural changes of the oligonucleotide due to the formation of DNA−protein complexes, an initial DNA concentration of 12 μM was titrated with protein and buffer to obtain molar ratios between DNA and protein from 0.5 to 1.5. Difference spectra were obtained by subtracting the pure protein spectra from the corresponding DNA−protein complex spectra.

All fluorescence spectra were measured at room temperature with a detector sensitivity of 450 V, an excitation bandwidth of 5 nm, an emission bandwidth of 10 nm, a data pitch of 1 nm, and two accumulations. The emission and excitation spectra of the pure carboxyfluorescein and Atto 550-labeled proteins, respectively, were measured at an excitation wavelength of 488 and 554 nm and an emission wavelength of 524 and 579 nm, respectively. Emission spectra of the protein−DNA complexes were recorded at an excitation wavelength of 470 nm. The initial DNA concentration was 12 μM. Protein solution (1:1 molar ratio of PhoB-CF and PhoB-Atto550) or buffer was added to obtain ratios between DNA and protein from 1 to 3.

SPR Measurements. All details concerning SPR have been described previously.[14]

Force Spectroscopy. Sample surface and AFM tip modification, as well as force spectroscopy measurements were performed as previously described.[17]

RESULTS AND DISCUSSION

Investigation of PhoB^{DBD} Point Mutants by Surface Plasmon Resonance and AFM Based Dynamic Force Spectroscopy Experiments. In order to compare single-molecule data (AFM-DFS) and macroscopic data (SPR), the point mutants R176A, T217A, V218A, and Y223A were analyzed by CD spectroscopy, SPR, and AFM-DFS. The corresponding amino acids exclusively interact with the minor groove of the *pho* box. CD spectroscopy was used to detect structural differences between WT-PhoB^{DBD} and all point mutants. The data are all in good agreement and indicate that all proteins exhibit a similar structure (cf. Figure S3 D).

The interaction between the point mutants and the oligonucleotides *MmMm* and *MmXx*, respectively, that either contain the entire *pho* box with the native major groove (*M*) and minor groove (*m*) sequences (cf. Table 2) or a randomized major groove (*X*) and minor groove (*x*) *pho* box, respectively, was quantified by surface plasmon resonance. Every SPR measurement was performed in duplicate to demonstrate the reproducibility (cf. Figure S4). Details concerning the optimization of the oligonucleotide design, the immobilization and the measurement procedure have already been published.[14] Although kinetic data like the dissociation rate constant k_{off} can in principle be derived from the SPR sensograms by fitting response curves to different kinetic models using a nonlinear least-squares algorithm, this direct analysis did not result in a reliable fit. One reason might be the fast association and dissociation of the PhoB^{DBD} that results in SPR curves characterized by a steep slope at the beginning and at the end of the injection.[14] Therefore, all dissociation constants were determined using the equilibrium response at different ligand concentrations. Like in the case of the alanine PhoB^{DBD} mutants of the amino acids aspartic acid 196 and arginine 219,[14] binding of the point mutants R176A and Y223A to the *pho* box is abolished. Replacing threonine 217 by alanine leads to a PhoB^{DBD} mutant that recognizes the *pho* box with an equilibrium dissociation constant increased by a factor of nearly 60 (K_D = 29.8 μM; cf. Figure 2) in comparison to WT-PhoB^{DBD} (K_D = 1.4 μM[14]). Moreover, if the second binding site of the *pho* box is additionally exchanged by a randomized sequence (*MmXx*), binding of PhoB^{DBD}T217A is nearly completely abolished (cf. Figure 2 B). In contrast to the PhoB^{DBD}-epitopes described so far, binding of PhoB^{DBD}V218A to the complete *pho* box is only marginally decreased by a factor of approximately 4 (K_D = 6.0 μM; cf. Figure 2). The complex consisting of PhoB^{DBD}V218A and the oligonucleotide *MmXx* exhibits an equilibrium dissociation constant of 37.9 μM. This value is increased by a factor of 1.7 in comparison to the corresponding result of WT-PhoB^{DBD} (K_D = 21.9 μM[14]). In the context of the information provided by the published X-ray and NMR structure of the protein−DNA complex,[1,9] the analysis of the binding behavior of the alanine mutants provide valuable insight into the types of interactions involved in the recognition process. Residues arginine 176, threonine 217, and tyrosine 223 interact with the minor groove by electrostatic interactions and hydrogen bonds, respectively. Additionally, threonine 217 binds to the DNA backbone by hydrophobic interactions.[9] One important discrepancy between the three amino acids that might explain the differences concerning the SPR results, is an intramolecular interaction. Arginine 176 and tyrosine 223 also interact with each other to stabilize the orientation and providing an optimal distance between helix α^2 and the C-terminal hairpin.[1] Therefore, DNA binding is completely disrupted if the two residues are mutated to alanine. Valine 218 also interacts with the minor groove by a hydrogen bond, formed between a water molecule and the carbonyl oxygen of the α-carboxyl group of the amino acid. The carboxyl group − and consequently also the corresponding interaction − is still present in the case of the mutated variant. Hence, no direct protein−DNA interactions should be affected. Still, valine 218 also mediates protein−protein interactions as part of a hydrophobic cluster. The amino acid is involved in the interactions between the C-terminal hairpin of the PhoB^{DBD} located upstream and the

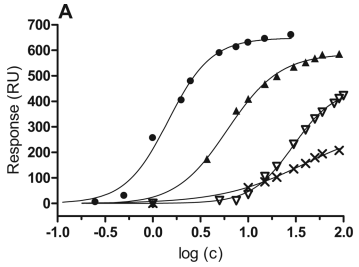

B

Protein : DNA complex		SPR K_D [μM]	SPR CI [μM]	SPR R^2	DFS k_{off} [s^{-1}]
WT-PhoB^{DBD} : *MmMm*	●	1.4	1.2-1.7	0.99	0.0025 ± 0.0021
WT-PhoB^{DBD} : *MmXx*	(13, 16)	21.9	10.3-33.4	0.99	
R176A : MmMm		---	---	---	1.873 ± 1.2
T217A : MmMm	▽	29.8	27.1-32.4	0.99	0.5337 ± 0.2
T217A : MmXx		---	---	---	
V218A : MmMm	▲	6.0	5.5-6.5	0.99	0.1432 ± 0.35
V218A : MmXx	x	37.9	30.2-45.7	0.99	
Y223A : MmMm		---	---	---	0.4514 ± 0.32

Figure 2. (A) Plotting the response units at equilibrium against the logarithm of the corresponding analyte concentrations gives saturation curves to derive the equilibrium dissociation constants using nonlinear regression. (B) Parameters of the complexes consisting of WT-PhoB^{DBD}, the PhoB^{DBD} point mutants, and the DNA molecules *MmMm* and *MmXx* derived from the SPR and DFS results: K_D = equilibrium dissociation rate constant (CI = 95% confidence interval), k_{off} = dissociation rate constant.

N-terminal β sheet of the second PhoB^{DBD} located downstream.[1] This explains the slightly increased equilibrium dissociation constants for the alanine mutant. Moreover, it becomes obvious why mutating valine 218 to alanine has a stronger effect on the recognition process of the oligonucleotide *MmMm* (K_D increased by a factor of 4 in comparison to *MmXx* that exhibits a K_D increased by a factor of 1.7). Only in the case of a complete *pho* box will extensive protein−protein interactions further stabilize the overall protein−DNA complex.[1]

The AFM-DFS results for the interaction between the PhoB^{DBD} point mutants and the *pho* box DNA (268 bp *pstS pho* box) are summarized in Figure 2B (DFS force versus loading rate plots: cf. Figure S5). All data are in good agreement with the SPR results described above. The dissociation rates of the complexes are significantly increased in comparison to the dissociation rate constant of the WT-PhoB^{DBD}-DNA complex. Moreover, the trend of the contributions of the investigated amino acids revealed by SPR is also in accordance with the DFS results. However, in contrast to the SPR data, even weak interactions could be quantified by DFS. Hence, the single-molecule data offer a more detailed differentiation of the amino acid contributions. In this context the DFS data indicate that arginine 176 seems to be the most important amino acid among the ones investigated. This aspect is in good agreement with the theory of Rohs et al., that positively charged amino acids, mainly arginine, primarily contribute to the interaction with the minor groove region.[19] Notably, the dissociation rate constant of the complex consisting of the *pho* box oligonucleotide and the point mutant V218A determined by AFM-DFS is also significantly increased, although the interaction between one protein and one DNA molecule and not the trimeric complex would be detected in these experiments. Valine 218 is supposed to mainly mediate protein−protein interactions. Such stabilizing effects due to protein−protein interactions should not be detected in the case of single-molecule methods. Taking this aspect of DFS into account, two explanations for the increased dissociation rates are possible: (1) Valine 218 mediates further direct interactions between the protein and the DNA aside from the hydrogen bond among the oligonucleotide and the amide group of the amino acid. (2) Structural differences between the point mutant and the WT-PhoB^{DBD} exist due to the mutations that were not visible by CD spectroscopy influencing DNA recognition. In conclusion, both methods complement each other: AFM-DFS leads to a more detailed differentiation of the contribution of amino acids for the overall recognition process, whereas SPR enables the investigation of further effects like protein−protein interactions. The combination of both methods enables quantification and discrimination between four types of contributions to the recognition process of the *pho* box by the protein PhoB^{DBD}: (1) interactions between positively charged amino acids and minor grooves with a high negative electrostatic potential (e.g., arginine 176); (2) direct interactions between the protein and the oligonucleotide mediated by hydrogen bonding in combination with the stabilization of the appropriate orientation of protein regions due to intramolecular interactions (e.g., arginine 176 and tyrosine 217); (3) direct protein−DNA recognition due to hydrogen bonds and hydrophobic interactions (e.g., threonine 217); (4) stabilization of the overall complex due to protein−protein interactions (e.g., valine 218).

Isothermal Titration Calorimetry. Binding of WT-PhoB^{DBD} to the oligonucleotide *MmMm* was investigated using ITC in order to get more information about the binding stoichiometry and the binding mechanism. The raw ITC data indicate an exothermic process (cf. Figure 3). The integrated heat values were fitted with a one-site binding model to obtain a binding stoichiometry of $n = 2.14 \pm 0.024$, an equilibrium dissociation constant of $K_D = 1.19 \pm 0.11$ μM, an enthalpy change of $\Delta H = -22.15 \pm 0.32$ kJ mol^{-1}, and an entropy change of $\Delta S = 39.23$ J mol^{-1} K^{-1} (cf. Figure 3). The stoichiometry of

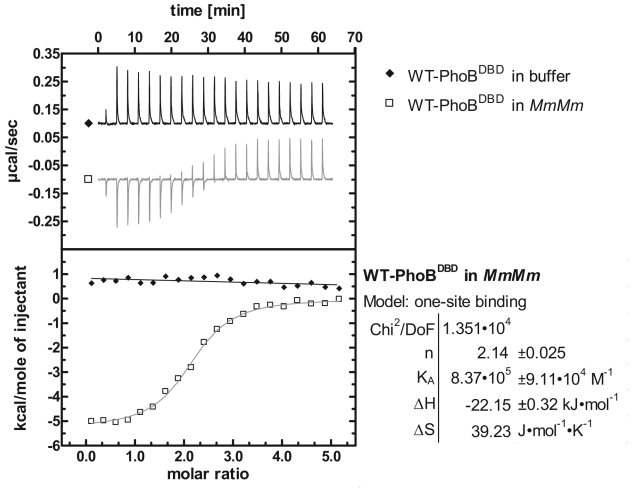

Figure 3. Isothermal calorimetric titration of *MmMm* with WT-PhoB^{DBD}. The upper panel shows the ITC raw data of the blank titration (WT-PhoB^{DBD} titrated into buffer) and the actual measurement (WT-PhoB^{DBD} titrated into buffer containing the DNA *MmMm*). The lower panel shows the integrated heats of binding (the blank was subtracted in the case of the actual measurement). The one-site binding model from MicroCal Origin was fitted to the data of the actual measurement (solid line).

dx.doi.org/10.1021/bi400718r | *Biochemistry* 2013, 52, 8177−8186

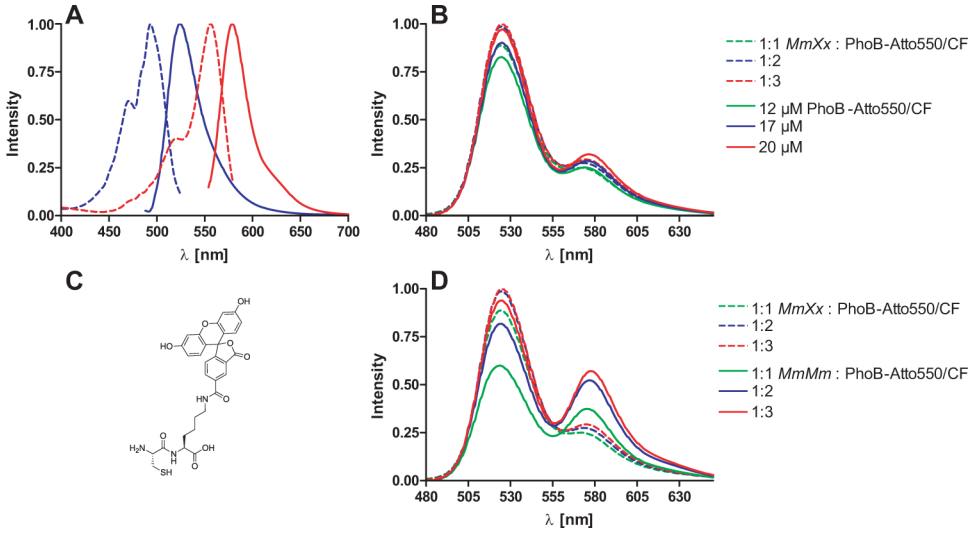

Figure 4. (A) Emission and excitation spectra of the pure proteins PhoB-CF (blue) and PhoB-Atto 550 (red) (excitation wavelengths: 488 and 554 nm, emission wavelengths: 524 and 579 nm). (B) Emission spectra of 1:1 mixtures of the proteins PhoB-CF and PhoB-Atto550 at different concentrations (the concentration equals the amount of protein in the protein−DNA complexes) and the protein−DNA complexes consisting of different ratios of protein (1:1 mixture of PhoB-CF and PhoB-Atto550) and the oligonucleotide *MmXx* (emission wavelength: 470 nm). (C) Structure of the carboxyfluorescein-labeled, cysteine containing peptide. (D) Emission spectra of the protein−DNA complexes consisting of different ratios of protein (1:1 mixture of PhoB-CF and PhoB-Atto550) and the oligonucleotide *MmMm*. For comparison, the spectra of the protein−*MmXx* complexes are displayed once more (emission wavelength: 470 nm).

approximately 2 indicates that both recognition sites of the *pho* box can be occupied by WT-PhoB^{DBD} molecules. Although a stoichiometric ratio of *MmMm* to WT-PhoB^{DBD} of 1:2 was detected, the only suitable model to evaluate the ITC data is a one-site binding model. These data and the equilibrium dissociation constant are both in perfect agreement with the results derived from the published SPR measurements (one-site binding; K_D = 1.4 μM; CI = 1.0−1.8 μM[14]). How would a one-site binding model be compatible with the formation of a trimeric complex?

FRET Experiments. FRET experiments were applied in order to gain more details regarding the binding mechanism of WT-PhoB^{DBD}. Two differently labeled proteins tagged with the FRET-donor carboxyfluorescein (CF) and the FRET-acceptor Atto 550, respectively, were prepared for this purpose. Titrating the native *pho* box (oligonucleotide *MmMm*) with a 1:1 mixture of the two proteins should result in a significant energy transfer because a trimeric complex consisting of the two PhoB^{DBD} and the DNA molecule is formed. In contrast, in the case of a partially randomized *pho* box (oligonucleotide *MmXx*) that only exhibits a single binding site with a 1:1 mixture no FRET should be detectable, because only a single protein can specifically address the oligonucleotide. The preparation of the CF-labeled protein started with the synthesis of a short CF-tagged cysteine containing peptide by solid phase peptide synthesis (SPPS). The structure of the peptide facilitates a high flexibility of the fluorescent label and thereby prevents that the PhoB^{DBD}-dimer formation is hindered during the recognition process due to the steric demand and hydrophobicity of the dye (cf. Figure 4C). In the following step, IPL was used to ligate the CF-labeled peptide specifically and quantitatively with the C-terminus of the WT-PhoB^{DBD} protein. Subsequently the newly introduced thiol group was reduced and masked using a mixture of TCEP and iodoacetamide to prevent the formation of disulfide bridged dimers. In order to obtain the Atto 550-labeled protein, amino acid glutamine 135 of the WT-PhoB^{DBD} was mutated to cysteine and the point mutant was incubated with Atto 550 maleimide. Residue 135 was chosen as ligation site due to the good accessibility and the fact that glutamine 135 is not involved in protein−protein or protein−DNA interactions.[1,9] Moreover, due to the position of the amino acid, no problems caused by steric hindrance should occur. The success of the preparation of both labeled proteins was proven by MALDI-ToF MS (cf. S1) and SDS-PAGE (cf. Figure S6). Maxima and minima of the excitation and emission spectra of the two PhoB^{DBD} are in good agreement with the specifications of the pure dyes (cf. Figure 4 A). Moreover, the results were used to calculate a Förster distance of R_0 = 6.6 nm for the CF-Atto 550 FRET-pair according to the literature known equations of the theory for resonance energy transfer.[20] The distance between both dyes accounts for approximately 3.5 nm in the trimeric complex regarding the crystal structure results.[4] Therefore, the calculated Förster radius value indicates that appropriate dyes were chosen for this FRET application. CD spectra of the labeled proteins and WT-PhoB^{DBD} were recorded to exclude influences on the protein structure by the fluorescence dyes (cf. Figure S3 E). The corresponding results show that all three proteins exhibit similar structures. Both labeled proteins were mixed in a molar 1:1 ratio for the FRET experiments. The oligonucleotides *MmMm* or *MmXx* were titrated with the protein-mixture to obtain oligonucleotide:-protein ratios of 1:1, 1:2, and 1:3. The corresponding emission spectra are given in Figure 4 B and D. In all cases, the maxima at 530 and 580 nm correspond to the CF- and Atto 550-labeled PhoB^{DBD} proteins, respectively. Two aspects complicate the quantification of the energy transfer. First of all, the excitation spectra of the two labeled PhoB^{DBD} partially overlap (the spectra of the two dyes are not baseline separated) and thereby adulterate the exact intensities. Moreover, each heterotrimeric protein−DNA complex has a certain statistical probability to consist of two PhoB^{DBD} with the same or with two different fluorescent labels. Therefore, all results can only be discussed in a qualitative manner. Comparing the emission spectra of the titration of the oligonucleotide *MmXx* with the results of the

dx.doi.org/10.1021/bi400718r | *Biochemistry* 2013, 52, 8177−8186

titration of pure buffer shows that no significant differences are visible (cf. Figure 4 B). Small variations in the intensity at 530 nm are due to unspecific quenching effects. Taking into consideration that FRET is distance dependent, no specific energy transfer can occur, since only one single protein can bind to the DNA molecule *MmXx*. In contrast, titrating *MmMm* with the protein-mixture leads to a significant reduction of the carboxyfluorescein intensity and a significant increase of the Atto 550 fluorescence (cf. Figure 4 D). In this case, a specific FRET occurs, because two proteins can interact with the oligonucleotide *MmMm*. Remarkably, a distinct FRET is already detectable in the presence of 1 equiv of protein. If the majority of *MmMm* would be occupied by a single PhoB^{DBD}-protein under these conditions, an emission spectrum that lacks a specific FRET should be detected in accordance with the results of *MmXx* (cf. Figure 4). Hence, the results of the fluorescence titration experiments indicate that the hetero-trimeric complex consisting of two PhoB^{DBD} and a single *MmMm* is already predominantly formed at substoichiometric protein concentrations (cf. Figure 4). Increasing the protein amount from an oligonucleotide:protein ratio of 1:2 to 1:3 results in an insignificant gain of the intensity at 580 nm, since all binding sites are already saturated at a ratio of 1:2 (cf. Figure 4 D).

Preparation and Characterization of PhoB^{DBD}-Dimers. Two different covalently linked PhoB^{DBD} dimers were prepared and the corresponding protein−DNA complexes investigated to elucidate the effect of dimerization on the binding mechanism and the complex stability. The first one, CRA-PhoB^{DBD}-dimer, contains the three amino acids cysteine, arginine, and alanine, that bridge the distance between the two DNA-binding domains (cf. Figure 5 B). Insertion of the three amino acids into the existing WT-PhoB^{DBD} structure (cf. Figure 5 A) and applying a Dreiding-like forcefield to this novel linker region and the surrounding amino acids reveals that the linker should not prevent the simultaneous interaction of the dimer with both recognition sites of a *pho* box (cf. Figure 5 B). A second dimer was designed that exhibits the amino acid sequence H-CRA-LEAF-OH as linker region to further increase the flexibility of the system. The theoretical consideration of the resulting complex consisting of CRA-LEAF-PhoB^{DBD}-dimer and the *pho* box indicates a less strained system (cf. Figure 5 C).

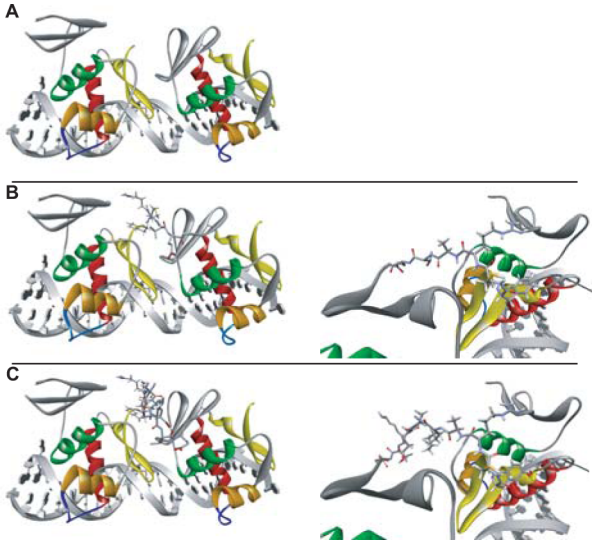

Figure 5. (A) Crystal structure of two WT-PhoB^{DBD} interacting with an 18 bp double-stranded *pho* box in a head-to-tail arrangement. (B, C) The crystal structure was expanded by the CRA- and the CRA-LEAF amino acid sequence, respectively. In both cases the structure of the two linker regions and the surrounding amino acids in between the monomeric PhoB^{DBD} was optimized using a fast, Dreiding-like forcefield (*Discovery Studio* v 3.5.0.12158, Accelrys).

Both dimers were prepared by native chemical ligation by fusing both cysteine epitopes (CRA-PhoB^{DBD} and CRA-LEAF-PhoB^{DBD}) to the C-terminus of an intein tag. After purification, both proteins exclusively exhibited an N-terminal cysteine residue and lacked the *N*-formylmethionine. Addition of both proteins to the MESNA-thioester of WT-PhoB^{DBD} resulted in the formation of the desired dimers by intein-mediated protein ligation (IPL). Both products precipitated during the ligation step. Denaturation using urea and masking the newly introduced thiol groups with a mixture of TCEP and iodoacetamide followed by renaturation by dialysis and purification by size exclusion chromatography provided CRA-PhoB^{DBD}-dimer and CRA-LEAF-PhoB^{DBD}-dimer in good purity. Success of the dimer formation was proven by MALDI-ToF MS (cf. S1) and SDS-PAGE (cf. Figure S7). Moreover, peptide mass fingerprinting analysis after tryptic digestion proved that the remaining bands belong to the two dimers (cf. S2). The corresponding results reveal sequence coverages of 96.7% (CRA-PhoB^{DBD}-dimer) and 97.2% (CRA-LEAF-PhoB^{DBD}-dimer). In conclusion, both dimers were successfully prepared using IPL.

CD spectroscopy was applied to verify that the two PhoB^{DBD}-dimers were properly refolded. An overlay of the corresponding CD spectra and percentages of secondary structure elements as calculated from all spectra using Yang's reference[21] indicate that CRA-PhoB^{DBD}- and CRA-LEAF-PhoB^{DBD}-dimer and the monomeric WT-PhoB^{DBD} exhibit similar structures (cf. Figure S3 A). Moreover, temperature dependent CD spectra of both dimers were recorded to estimate the temperature of heat denaturation. CRA-PhoB^{DBD}- and CRA-LEAF-PhoB^{DBD}-dimer denature at 45.5 and 42.4 °C, respectively, indicating that both proteins exhibit a similar stability (cf. Figure S3 B, C). In conclusion, all CD spectra verify that the two PhoB^{DBD}-dimers CRA-PhoB^{DBD}- and CRA-LEAF-PhoB^{DBD}-dimer are properly folded. CD spectroscopy was also used to investigate the DNA recognition characteristics of both PhoB^{DBD}-dimers. In order to reveal structural changes of the oligonucleotide upon formation of the protein−DNA complex, differential CD spectra were obtained by subtracting the protein spectra from the corresponding complex spectra at different protein−DNA ratios. All DNA spectra are characterized by a positive band at 275 nm and a negative band at 248 nm with comparable intensities (cf. Figure 6 A-C). The maximum results from the base stacking and the minimum is characteristic for a right-handed B-DNA duplex.[22,23] We recently reported that the recognition of a complete *pho* box that exhibits two neighboring binding sites (oligonucleotide *MmMm*) by two WT-PhoB^{DBD} results in a structural change of the oligonucleotide due to DNA bending (cf. Figure 6 A). However, no structural change is detectable by CD spectroscopy, if an oligonucleotide comprising only one single binding site is applied.[14,17] The CD results corresponding to the recognition of the complete *pho* box by the two PhoB^{DBD}-dimers indicate that the oligonucleotide is bent upon complex formation in both cases. Remarkably, increasing the protein-dimer amount from 1 to 1.5 equiv does not result in a further change of the CD effect (cf. Figure 6 B, C), since all binding

dx.doi.org/10.1021/bi400718r | *Biochemistry* 2013, 52, 8177−8186

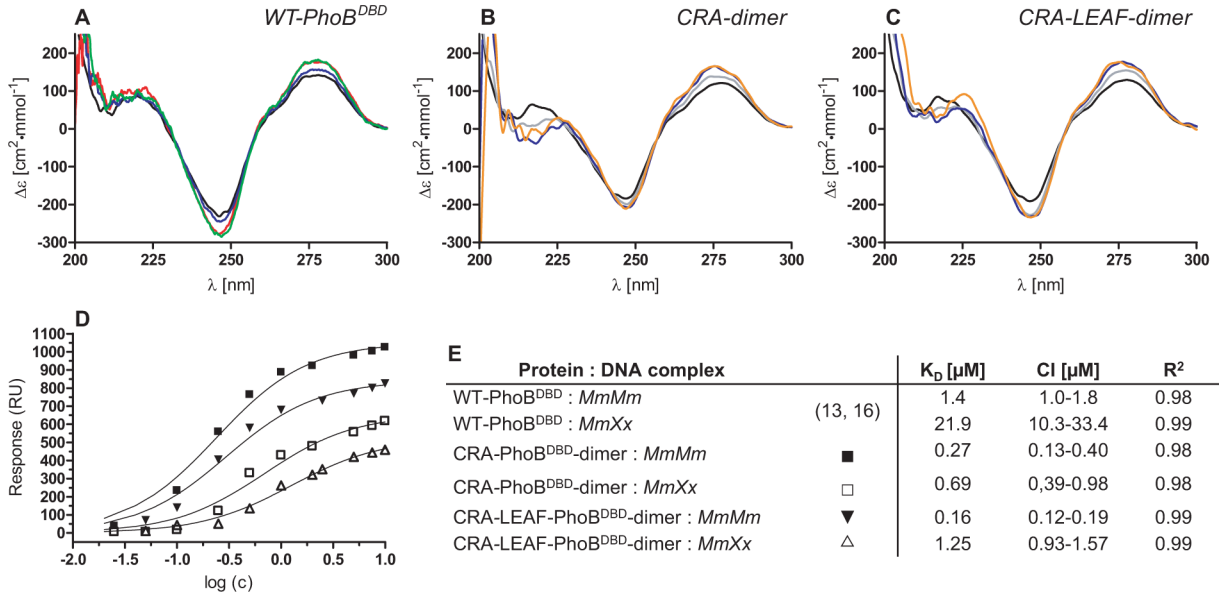

Figure 6. (A-C) Differential CD spectra of WT-PhoB^{DBD}- and PhoB^{DBD}-dimer−*MmMm* complexes minus protein spectra at different ratios. Color code: (black) DNA:PhoB^{DBD} 1:0, (gray) DNA:PhoB^{DBD} 1:0.5, (blue) DNA:PhoB^{DBD} 1:1, (yellow) DNA:PhoB^{DBD} 1:1.5, (red) DNA:PhoB^{DBD} 1:2, and (green) DNA:PhoB^{DBD} 1:3. (D) Plotting the response units at equilibrium against the logarithm of the corresponding analyte concentrations gives saturation curves to derive the equilibrium dissociation constants using nonlinear regression. (E) Parameters of the complexes consisting of the two PhoB^{DBD}-dimers and the DNA molecules *MmMm* and *MmXx* derived from the SPR results: K_D = equilibrium dissociation rate constant (CI = 95% confidence interval).

sites are already saturated. In conclusion, the CRA-PhoB^{DBD}- and the CRA-LEAF-PhoB^{DBD}-dimer recognize the *pho* box as dimers with a stoichiometry of 1:1. This result shows that both linkers align the two PhoB^{DBD} units at an appropriate distance. Comparing the differential CD spectra of the three protein−DNA complexes, especially at a wavelength of 275 nm, further reveals that increasing the protein amount from 0 to 1 equiv in the case of WT-PhoB^{DBD} monomer and from 0 to 0.5 equiv in the case of both dimers results in a comparable structural change of the oligonucleotide. These data support the results of the FRET experiments that even in the presence of only 1 equiv of WT-PhoB^{DBD} an excess of complexes is composed of one DNA molecule and two proteins.

SPR experiments were performed to quantify DNA recognition by the two covalent PhoB^{DBD}-dimers. The complexes consisting of the oligonucleotide *MmMm* and the two dimers CRA-PhoB^{DBD} and CRA-LEAF-PhoB^{DBD}, respectively, are characterized by K_D values of 0.27 and 0.16 μM (cf. Figure 6 D, E). Hence, both values are reduced by a factor of 5−10 in comparison to the equilibrium dissociation constant of the complex consisting of *MmMm* and WT-PhoB^{DBD} (K_D = 1.4 μM). This result reveals that the covalent dimerization essentially promotes the complex stability. Furthermore, the two K_D values of the two dimer-complexes differ by a factor of 1.7. Thus, increasing the length of the linker region in between the two PhoB^{DBD} further enhances the stability of the protein−DNA complex. The complexes consisting of both dimers (CRA-PhoB^{DBD} and CRA-LEAF-PhoB^{DBD}) and the oligonucleotide *MmXx* with a single binding site are characterized by equilibrium dissociation constants of 0.69 and 1.25 μM, respectively (cf. Figure 6 D, E). The reduction of both values by a factor of approximately 20 in comparison to the dissociation constant of the WT-PhoB^{DBD} complex (K_D = 21.9 μM) can be explained by nonspecific interactions between the second DBD of the two dimers and the randomized DNA region adjacent to the recognition site of the DNA molecule *MmXx*. Another possible explanation is based on an increased rebinding rate of all dissociating proteins to the recognition site due to the existence of two cross-linked DBD.

Phosphorylation of full-length PhoB in the regulatory domain PhoBRD significantly shifts the monomer−dimer equilibrium to the dimeric form and results in a structural change where the two DBDs can bind to a *pho* box in a parallel head-to-tail arrangement.[12,13] The impact of phosphorylation and the resulting increase of PhoB-dimers was quantified by fluorescence anisotropy measurements. McCleary et al. determined values of 4.3 μM in the case of the inactive form and 0.49 μM in the case of the phosphorylated form of PhoB.[24] Mack et al. obtained equilibrium dissociation constants of 145 nM and 9.7 nM for the dephosphorylated and phosphorylated form of the entire transcriptional activator, respectively.[13] Although these values differ by several orders of magnitude, it has to be taken into consideration that different *pho* box sequences were investigated. Still, the results of McCleary et al. and Mack et al. indicate that the equilibrium dissociation constant is reduced by a factor of 10−15 upon phosphorylation and dimerization. This aspect is in good agreement with the results presented here. Hence, dimerization of two WT-PhoB^{DBD} decreases the equilibrium dissociation constant of the corresponding protein−DNA complex by a factor of approximately 10, with the two DNA binding domains either dimerized by the phosphorylated PhoBRD or linked covalently. This result emphasizes the significance of dimerization and indicates that the regulatory domain of full-length PhoB can be easily substituted by a three amino acid based linker that keeps the two PhoB^{DBD} in the right orientation.

Binding Mechanism of PhoB^{DBD}. The ITC results prove that the complex consisting of *MmMm* and WT-PhoB^{DBD} is characterized by a stoichiometric ratio of 1:2 (cf. Figure 3). The SPR and AFM-DFS results of the PhoB^{DBD} point mutants

dx.doi.org/10.1021/bi400718r | *Biochemistry* 2013, 52, 8177−8186

further reveal that protein−protein interactions and the correct orientation of involved protein regions extensively contribute to the stability of the heterotrimeric complex aside from electrostatic interactions and hydrogen bonds (cf. Figure 2). Thus one would expect a cooperative two-site binding mechanism. Still, the only suitable model to characterize the recognition process and evaluate the ITC and SPR data is a one-site binding model. There are three possible explanations:

1. Two Identical, Noninteracting Binding Sites Exist. The SPR results indicate that both binding sites exhibit comparable affinity for WT-PhoB^{DBD}.[14] However, the formation of the heterotrimeric complex consisting of two WT-PhoB^{DBD} and a single *pho* box (*MmXx*) results in a K_D value reduced by almost 15−20 μM. Hence, protein−protein interactions definitely stabilize the complex.

2. WT-PhoB^{DBD} is Already a Dimer before Binding to Pho Box Promoters. Coll and co-workers mention size-exclusion chromatography experiments indicating that the DNA-binding domain PhoB^{DBD} exclusively exists as a dimer.[25] However, during the purification of the covalently linked dimers CRA-PhoB^{DBD}- and CRA-LEAF-PhoB^{DBD}-dimer by gel filtration chromatography the PhoB^{DBD}-monomers were successfully removed (cf. Figure S7). Furthermore, the FRET results reveal that the energy transfer is significantly increased only in the presence of a complete *pho* box (cf. Figure 3 B-D). If WT-PhoB^{DBD} would exclusively exist in a dimeric form in solution, these noncovalently dimerized monomers would have been coeluted with the cross-linked PhoB^{DBD}-dimers during the purification step and the formation of PhoB^{DBD}-*MmMm* complexes would not result in a significant increase of the Atto 550 fluorescence in the case of the FRET experiments. Thus, our results exclude permanent dimer formation.

3. Binding Occurs with Infinite Positive Cooperativity—1:1 Complexes Are Not Resolvable. The population of the heterodimeric 1:1 species depends on the relative values of the equilibrium dissociation constants for each of the two steps. In the case of an infinite cooperativity, the concentration of the intermediate 1:1 complex is negligibly low in comparison to the concentration of the final heterotrimeric 2:1 protein−DNA complex. The results of the fluorescence titration experiment (cf. Figure 4 B-D) verify, in accordance with the differential CD results (cf. Figure 6 A-C), that trimeric complexes of two PhoB^{DBD} molecules already exist at low protein concentrations. These data support a completely cooperative binding mechanism. Fitting the equilibrium response of the SPR experiments at different ligand concentrations using the Hill equation (cf. eq 1) for two equivalent recognition sites permits the quantification of the cooperative effect:[26]

$$R_{eq} = \frac{B_{max}[\text{PhoB}^{DBD}]^h}{K_D^h + [\text{PhoB}^{DBD}]^h} \quad (1)$$

In this equation, h is the Hill coefficient, R_{eq} the equilibrium response units B_{max} the maximum specific binding, and [PhoB^{DBD}] the analyte concentration. Re-evaluation of the SPR data of the interaction between WT-PhoB^{DBD} and the oligonucleotide *MmMm* by nonlinear regression using eq 1 indicates a Hill coefficient of h = 1.9 (cf. Table 3). Moreover, the complexes consisting of the two point mutants T217A and V218A, respectively, and the DNA molecule *MmMm* exhibit Hill slopes in the same range (h = 2.0 and 1.6, cf. Table 3). Taking into consideration that the stoichiometry and, therefore, also the maximum Hill coefficient would be h = 2, this result clearly proves that the recognition of the entire *pho* box by PhoB^{DBD} follows a completely positive cooperative binding mechanism. Thus, 1:1 complexes are not resolvable as they are not significantly populated.

Table 3. Hill Coefficients (h) Derived from the SPR Results According to Eq 1 Using Nonlinear Regression[a]

Protein:DNA complex	Hill slope (h)	CI
WT-PhoB^{DBD}:*MmMm*	1.9	1.4−2.0
T217A:*MmMm*	2.0	1.7−2.0
V218A:*MmMm*	1.6	1.3−1.8

[a] The corresponding K_D values and saturation curves are summarized in Figure 2. (CI = 95% confidence interval).

CONCLUSIONS

In this study, a combination of single-molecule and ensemble methods was used to investigate the binding mechanism and the impact of dimerization on the protein−DNA complex stability of PhoB^{DBD}. These insights can be translated to related members of the family of winged helix-turn-helix proteins. ITC data verify the published SPR results and indicate that a one-site binding model is the only suitable model, although a molar ratio of protein:DNA 2:1 is required. The results of the fluorescence resonance energy transfer experiments and the elucidation of the binding characteristics of covalently linked PhoB^{DBD}-dimers by CD spectroscopy and SPR verify that trimeric complexes of two PhoB^{DBD} molecules already exist at an excess of native *pho* box sequences. A re-evaluation of the surface plasmon resonance data of the quantification of the interaction between PhoB^{DBD} and *MmMm* by nonlinear regression using the Hill equation further indicates that the complex formation follows a completely positive cooperative binding mechanism. Thus, 1:1 complexes are not resolvable as they are not significantly populated. The results of the characterization of the covalently linked dimers also reveal that cross-linking two PhoB^{DBD} essentially promotes the protein−DNA complex stability with respect to the flexibility of the investigated dimer. Comparing these data with the equilibrium dissociation constants published for the interaction of phosphorylated and unphosphorylated full length PhoB with *pho* box oligonucleotides leads to the conclusion that dimerization decreases the K_D value by a factor of approximately 10, independent of the dimerization method.

The contributions of the amino acids R176, T217, V218, and Y223 were investigated by both methods to compare the information content of the two techniques AFM-DFS and SPR and to distinguish between different types of binding. SPR and AFM-DFS complement one another: The single-molecule method provides a more detailed view on the contribution of amino acids for the overall recognition process, whereas SPR enables the investigation of further effects like protein−protein interactions. The application of both techniques in combination with available NMR and X-ray structure data can be used to create a dynamic picture of the protein−DNA interaction and to differentiate between four types of binding that contribute to the overall recognition process.

ASSOCIATED CONTENT

Supporting Information

Results from peptide mass fingerprinting analysis, SDS gels, CD spectra, SPR sensograms, DFS data. This material is available free of charge via the Internet at http://pubs.acs.org.

dx.doi.org/10.1021/bi400718r | *Biochemistry* 2013, 52, 8177−8186

AUTHOR INFORMATION

Corresponding Author

*Tel.: +49 521 106 2051, E-mail: Norbert.Sewald@uni-bielefeld.de.

Author Contributions

The manuscript was written through contributions of all authors. All authors have given approval to the final version of the manuscript.

Funding

This work was supported by the German Research Foundation (DFG, SFB 613) and the German National Academic Foundation (Studienstiftung des Deutschen Volkes, PhD fellowship to Markus Ritzefeld).

Notes

The authors declare no competing financial interest.

ACKNOWLEDGMENTS

Prof. Dr. Hartmut Niemann is acknowledged for helpful discussions.

ABBREVIATIONS

AFM, atomic force microscopy; RNAP, bacterial RNA polymerase; CF, carboxyfluorescein; CD, circular dichroism spectroscopy; $PhoB^{DBD}$, DNA-binding domain of PhoB; DFS, dynamic force spectroscopy; *E. coli*, *Escherichia coli*; FRET, fluorescence resonance energy transfer; IPL, intein-mediated protein ligation; ITC, isothermal titration calorimetry; SPPS, solid phase peptide synthesis; SPR, surface plasmon resonance; TCRS, two-component regulatory system

REFERENCES

(1) Blanco, A. G., Sola, M., Gomis-Rüth, F. X., and Coll, M. (2002) Tandem DNA Recognition by PhoB, a Two-Component Signal Transduction Transcriptional Activator. *Structure 10*, 701−713.

(2) Gajiwala, K. S., and Burley, S. K. (2000) Winged helix proteins. *Curr. Opin. Struct. Biol. 10*, 110−116.

(3) Teichmann, M., Dumay-Odelot, H., and Fribourg, S. (2012) Structural and functional aspects of winged-helix domains at the core of transcription initiation complexes. *Transcription 3*, 2−7.

(4) Yang, C., Huang, T.-W., Wen, S.-Y., Chang, C.-Y., Tsai, S.-F., Wu, W.-F., and Chang, C.-H. (2012) Genome-wide PhoB binding and gene expression profiles reveal the hierarchical gene regulatory network of phosphate starvation in *Escherichia coli*. *PLoS ONE 7*, e47314.

(5) Hsieh, Y.-J., and Wanner, B. L. (2010) Global Regulation by the seven-component Pi signaling system. *Curr. Opin. Microbiol. 13*, 198−203.

(6) Makino, K., Shinagawa, H., Amemura, M., and Nakata, A. (1986) Nucleotide sequence of the phoB gene, the positive regulatory gene for the phosphate regulon of *Escherichia coli* K-12. *J. Mol. Biol. 190*, 37−44.

(7) Yoshida, Y., Sugiyama, S., Oyamada, T., Yokoyama, K., and Makino, K. (2012) Novel members of the phosphate regulon in Escherichia coli O157:H7 identified using a whole-genome shotgun approach. *Gene 502*, 27−35.

(8) Wanner, B. L. (1993) Gene regulation by phosphate in enteric bacteria. *J. Cell. Biochem. 51*, 47−54.

(9) Yamane, T., Okamura, H., Ikeguchi, M., Nishimura, Y., and Kidera, A. (2008) Water-mediated interactions between DNA and PhoB DNA-binding/transactivation domain: NMR-restrained molecular dynamics in explicit water environment. *Proteins: Struct. Funct. Bioinformatics 71*, 1970−1983.

(10) Canals, A., Blanco, A. G., and Coll, M. (2012) σ70 and PhoB activator: getting a better grip. *Transcription 3*, 4−8.

(11) Blanco, A. G., Canals, A., Bernués, J., Solà, M., and Coll, M. (2011) The structure of a transcription activation subcomplex reveals how σ(70) is recruited to PhoB promoters. *EMBO J. 30*, 3776−3785.

(12) Bachhawat, P., Swapna, G. V. T., Montelione, G. T., and Stock, A. M. (2005) Mechanism of activation for transcription factor PhoB suggested by different modes of dimerization in the inactive and active states. *Structure 13*, 1353−1363.

(13) Mack, T. R., Gao, R., and Stock, A. M. (2009) Probing the roles of the two different dimers mediated by the receiver domain of the response regulator PhoB. *J. Mol. Biol. 389*, 349−364.

(14) Ritzefeld, M., Wollschläger, K., Niemann, G., Anselmetti, D., and Sewald, N. (2011) Minor groove recognition is important for the transcription factor PhoB: a surface plasmon resonance study. *Mol. BioSyst. 7*, 3132−3142.

(15) Ellison, D. W., and McCleary, W. R. (2000) The unphosphorylated receiver domain of PhoB silences the activity of its output domain. *J. Bacteriol. 182*, 6592−6597.

(16) Ritzefeld, M., Walhorn, V., Anselmetti, D., and Sewald, N. (2013) Analysis of DNA interactions using single-molecule force spectroscopy. *Amino Acids 44*, 1457−1475.

(17) Wollschläger, K., Gaus, K., Körnig, A., Eckel, R., Wilking, S.-D., McIntosh, M., Majer, Z., Becker, A., Ros, R., Anselmetti, D., and Sewald, N. (2009) Single-molecule experiments to elucidate the minimal requirement for DNA recognition by transcription factor epitopes. *Small 5*, 484−495.

(18) Ritzefeld, M., and Sewald, N. (2012) Real-time analysis of specific protein-DNA interactions with surface plasmon resonance. *J. Amino Acids 2012*, 1−19.

(19) Rohs, R., West, S. M., Sosinsky, A., Liu, P., Mann, R. S., and Honig, B. (2009) The role of DNA shape in protein−DNA recognition. *Nature 461*, 1248−1253.

(20) Lakowicz, J. R. (2010) *Principles of Fluorescence Spectroscopy*, 4th Printing, Springer, New York.

(21) Chen, Y. H., and Yang, J. T. (1971) A new approach to the calculation of secondary structures of globular proteins by optical rotatory dispersion and circular dichroism. *Biochem. Biophys. Res. Commun. 44*, 1285−1291.

(22) Ivanov, V. I., and Minyat, E. E. (1981) The transitions between left- and right-handed forms of poly(dG-dC). *Nucleic Acids Res. 9*, 4783−4798.

(23) Kypr, J., Kejnovska, I., Renciuk, D., and Vorlickova, M. (2009) Circular dichroism and conformational polymorphism of DNA. *Nucleic Acids Res. 37*, 1713−1725.

(24) McCleary, W. R. (1996) The activation of PhoB by acetylphosphate. *Mol. Microbiol. 20*, 1155−1163.

(25) Blanco, A. G., Canals, A., and Coll, M. (2012) PhoB transcriptional activator binds hierarchically to pho box promoters. *Biol. Chem. 393*, 1165−1171.

(26) Rippe, K. (1997) Analysis of protein-DNA binding at equilibrium. *B. F. Futura 12*, 20−26.